Sedimentology of a Late Quaternary lacustrine record from the south-eastern Carpathian Basin

Zeeden, C.; Hambach, U.; Klasen, N.; Fischer, P.; Schulte, P.; Nett, J.J.; ... ; Lehmkuhl, F.

JOURNAL OF QUATERNARY SCIENCE (2021) **36**(8) 1414–1425 ISSN 0267-8179. DOI: 10.1002/jqs.3297

JQS Journal of Quaternary Science QRA Quaternary Research Association

Sedimentology of a Late Quaternary lacustrine record from the south-eastern Carpathian Basin

CHRISTIAN ZEEDEN,[1,2]* ULRICH HAMBACH,[3] NICOLE KLASEN,[4] PETER FISCHER,[5] PHILIPP SCHULTE,[1] JANINA J. NETT,[1] DANIEL VERES,[6] IGOR OBREHT,[1,7] WEI CHU,[8] MARIA PAPADOPOULOU,[9] FINN VIEHBERG,[10] FRANK SCHÄBITZ,[9] MILIVOJ B. GAVRILOV,[11] SLOBODAN B. MARKOVIĆ,[11] ANDREAS VÖTT[5] and FRANK LEHMKUHL[1]

[1]Department of Geography, RWTH Aachen University, Germany
[2]Leibniz Institute for Applied Geophysics, Hannover, Germany
[3]BayCEER & Chair of Geomorphology, University of Bayreuth, Germany
[4]Institute of Geography, University of Cologne, Germany
[5]Institute for Geography, Johannes Gutenberg-Universität Mainz, Germany
[6]Institute of Speleology, Romanian Academy, Cluj-Napoca, Romania
[7]MARUM, University Bremen, Germany
[8]Institute of Prehistoric Archaeology, University of Cologne, Germany
[9]Institute of Geography Education, University of Cologne, Cologne, Germany
[10]Institute for Geography and Geology, Universität Greifswald, Germany
[11]Chair of Physical Geography, Faculty of Sciences, University of Novi Sad, Serbia

Received 30 September 2020; Revised 16 February 2021; Accepted 23 February 2021

ABSTRACT: The Upper Pleistocene geoarchives in the south-eastern Carpathian Basin are represented predominantly by loess–palaeosol records. In 2015, a 10 m sediment core composed of clay-rich lacustrine sediments was recovered by vibracoring a dry lake basin located between the Vršac Mountains (Serbia) and the Banat Sands in the south-eastern Carpathian Basin; a location relevant for placing regional archaeological results in a palaeoenvironmental context. Here, we present results from geoelectrical prospection and a lithostratigraphic interpretation of this sequence supported by a detailed granulometric study supplemented by ostracod analysis. An age model based on luminescence dating is discussed against sedimentological proxy data and its implication for palaeoenvironmental change. The cores show a stratigraphy of lighter ochre-coloured and darker greyish sediment, related to the deposition of clay and silt trapped in an aquatic environment. Geophysical measurements show ~20 m thick lacustrine sediments. The grain-size distributions including the variability in fine clay are indicative of a lacustrine environment. Fine particles were brought into the depositional environments by aquatic input and settled from suspension; also, direct dust input is constrained by grain-size results. Riverine input and aeolian dust input interplayed at the locality. © 2021 The Authors *Journal of Quaternary Science* Published by John Wiley & Sons, Ltd.

Introduction

The Carpathian Basin (Middle Danube Basin) is a key area to investigate the influence of the continental, Mediterranean and Atlantic climate interaction over Europe during the Quaternary (Stevens *et al.*, 2011; Obreht *et al.*, 2016). Large areas of the basin are covered by floodplain deposits and aeolian sediments (aeolian sands, loess, and loess-like sediments; Haase *et al.*, 2007; Lindner, 20120167; Lehmkuhl *et al.*, 2018, 2020). Investigating these aeolian sediments led to a better understanding of Quaternary palaeoclimate evolution (see e.g. Marković *et al.*, 2015). The understanding of past environmental conditions relevant for loess and loess-like sediments relies on biological proxies; in this area usually malacological assemblages (e.g. Marković *et al.*, 2007; Molnár *et al.*, 2010; Sümegi *et al.*, 2012a, 2013a), stable isotopes (Banak *et al.*, 2016) and n-alkanes. For an overview, see Obreht *et al.*, (2019). It is widely accepted that Late Pleistocene palaeoenvironments in the southern Carpathian Basin were dominated by open steppe grasslands, and partly forest steppes (Zech *et al.*, 2009; Sümegi *et al.*, 2012b; Marković *et al.*, 2007, 2018). Establishing the environmental conditions and dominating vegetation is still challenging. Also, constraining the exact timing of palaeoenvironmental changes is debated (Willis *et al.*, 2000; Rudner and Sümegi, 2001; Willis and van Andel, 2004). In contrast, lacustrine geoarchives can be excellent recorders of e.g., pollen and other biological proxies, thus allowing for more reliable palaeoenvironmental reconstructions. These are available for long and high-resolution sequences close to the Mediterranean region and in the mountain ranges of the southern Balkans, such as Tenagi Philippon (e.g. Tzedakis *et al.*, 2006; Pross *et al.*, 2015), Lake Ioannina, Lake Ohrid (e.g. Just *et al.*, 2019; Wagner *et al.*, 2019, and references therein) and Lake Prespa (Panagiotopoulos *et al.*, 2013). Unfortunately, only one long lacustrine record from the surrounding Carpathians exists, from Lake St. Ana in Romania (Magyari *et al.*, 2009, 2014; Tóth *et al.*, 2018), representing mainly mountain environments and does not span the entire last glacial cycle (Feurdean *et al.*, 2014). However, those records indicate a more complex environmental evolution of the Carpathian Mountains and adjacent areas during the last glacial cycle, with varying phases of grassland and forest domination (Sümegi *et al.*, 2013b). Therefore, the rising challenge is to connect the palaeoenvironmental conditions as inferred from lowland areas of the Carpathian Basin to the surrounding mountain areas of the Carpathian range (see also, Staubwasser *et al.*, 2018).

*Correspondence: C. Zeeden, Leibniz Institute for Applied Geophysics, as above.
Email: christian.zeeden@leibniz-liag.de

Until now, there are not many lacustrine or peat records (Sümegi *et al.*, 2011b, and references therein) from the lowland areas in the south-eastern Carpathian Basin reaching into the last glacial cycle, and most records are overbank or oxbow lake deposits related to the large river systems in the basin. However, several dry lake basins are present in the area around Vršac (Serbia) containing sediments deposited in palaeolakes and shallow swamps (Fig. 1). Here we present and discuss data highlighting the importance of one of these lacustrine geoarchives from the edge of the Carpathian Basin. Besides the lithostratigraphic core description, we present a chronology based on luminescence and radiocarbon dating, and grain-size data.

Understanding the Late Pleistocene environmental history of the Vršac Basin (Fig. 1) is archaeologically relevant due to its proximity to a number of important human fossils and early Upper Palaeolithic sites. Across the border in Romania (*c.* 55 km east), the Peștera cu Oase has yielded one of the earliest securely dated modern human fossils in Europe (*c.* 36–34 ka ^{14}C years BP, Trinkaus *et al.*, 2003, 2012) with Neanderthal admixture (Fu *et al.*, 2015). In and around the Vršac Basin, rich Aurignacian sites and find spots occur, namely Crvenka-At, Românești, Coșava, Temerești, Tincova and Tabula Traiana (Mihailović, 2011; Anghelinu *et al.*, 2012; Borić *et al.*, 2012; Sitlivy *et al.*, 2012, 2014; Chu *et al.*, 2014, 2016, 2019; Nett *et al.*, 2021). Given the ongoing discussion concerning the role of climate in Late Pleistocene population turnover in the region (Müller *et al.*, 2011; Staubwasser *et al.*, 2018; Alex *et al.*, 2019), the Vršac core may provide a valuable cross-check to local palaeoenvironmental reconstructions for late surviving Neanderthal populations and the earliest modern humans in Europe, as derived from loess data (Schmidt *et al.*, 2013; Kels *et al.*, 2014; Obreht *et al.*, 2017). It may also contribute to a better understanding of the postulated Danube catchment as a migration corridor towards central and western Europe (Chu, 2018, and references therein).

The aim of this study is to provide a stratigraphy and sedimentological and palaeoclimatological interpretation for the Late Quaternary evolution of the Vršac Basin, and place it in the context of loess geoarchives. In addition, the implications of palaeoenvironmental change in relation to human occupation in the area are discussed.

Study area

North and north-west of Vršac, several morphological depressions exist. These were occupied by lakes and swamps before their drainage in historical times (Timár *et al.*, 2008). Our coring was performed in the Alibunar Depression (see Fig. 1), which was described as a 'Morast' (German for mire/mud/swamp) in the historical map of Müller (1769). It was drained during the late 18th and early 19th centuries (Müller, 1769; Timár *et al.*, 2008). The depression is located between the loess and dune fields of the Banat Sands (Deliblatska Peščara) in the west, and the Vršac Mountains in the east. It is one of several oval landforms in the area; these have a maximal elevation of *c.* 75 m above mean sea level (amsl) and their maximal extent in west-south-west–east-north-east direction. They form endorheic basins and are the lowest points in the landscape, being ~10–15 m below separating ridges, and ~40 m (loess plateau at Alibunar) deeper than the surrounding geomorphological units. The depressions are separated by longitudinal positive landforms. The ridge south-east of our coring site consists of silt-dominated and partly gravelly, presumably fluvial, overbank deposits, turning to sandy and gravel deposits downwards (Nett *et al.*, 2021). From a tectonic point of view, the area under investigation is part of a dextral transpressive wrenching system bordering the Carpathian Basin in the south and creating closely neighbouring subsidence and uplift structures (Horváth *et al.*, 2015; Sušić *et al.*, 2016). The still ongoing Neogene subsidence was in the order of 1–2 km in this area (Marović *et al.*, 2007), and the Quaternary deposits reach thicknesses of about 450 m in the northern Serbian Banat (Pigott and Radivojević, 2010). Observed west-south-west/east-north-east striking oval forms north-west of Vršac cut into loess deposits in the west and to a minor extent in the east, suggesting that the erosion connected

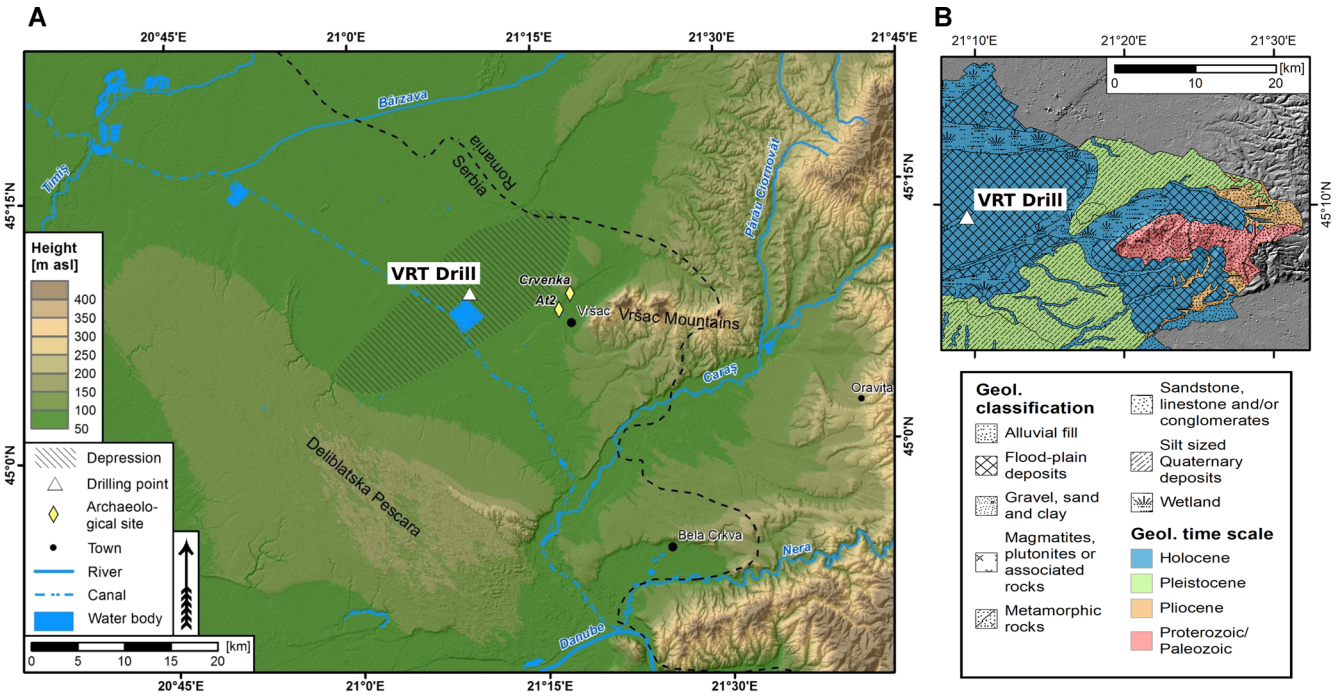

Figure 1. (A) Study area in north-eastern Serbia (white triangle: drill Site) in geographical context. (B) highlights the local geology, where colours encode time and patterns represent different rock types and sedimentary environments. [Color figure can be viewed at wileyonlinelibrary.com].

to the maximum water tables in these depressional landforms post-date the last phase of massive loess accretion. The genesis of the Vršac Mountains with their steep northern flanks and relatively gentle southern slopes is bound to the Neogene tectonic activity as well (e.g. Matenco and Radivojević, 2012).

The Banat Sands in the south-west of the study area represent a vast body of aeolian transported deposits with longitudinal landforms (Fig. 1A), indicating general sediment input from the south-east including the Danube floodplain (Gavrilov *et al.*, 2018). A loess ridge reaching maximum elevation of *c.* 250 m amsl borders the Banat Sands to the north-east. Between this ridge and the here focused depression, the landscape is covered by loess, exhibiting a surface gently dipping towards the north-east from ~150 m to ~100 m to the rim of the depression (Fig. 1A). The south-eastern aeolian dust transport direction, as indicated by morphology of the Banat Sands, may play a role in larger parts of the south-eastern Carpathian Basin (Zeeden *et al.*, 2007; Barbu *et al.*, 2009; Obreht *et al.*, 2015), and is probably related to the influence of the south-east wind (locally known as the Coşava or Košava wind; Gavrilov *et al.*, 2018). Outside the depressions and the tectonic push-up structures like the Vršac Mountains and the ridges separating the depressions and surrounding the Banat Sands, a loess cover in plateau facies forms an aeolian blanket. In the southern Carpathian Basin, the last glacial cycle experienced high sedimentation rates of aeolian dust of *c.* 5–15 cm/ka in most places (see, e.g. Buggle *et al.*, 2009; Fitzsimmons *et al.*, 2012; Marković *et al.*, 2014; Fenn *et al.*, 2020), which decreases with increasing distance from the large river systems. The depressions near Vršac show a west-south-west/east-north-east orientation, and are therefore unlikely to be related to aeolian processes, since south-easterly winds were probably persistent at least from the Last Glacial Maximum (LGM; Gavrilov *et al.*, 2018). We interpret them to be linked to tectonic activity. This direction is also indicated by Marović *et al.* (2007) for faults in the area, underlining the tectonic origin of the depressions.

In the north-west of the Vršac Mountains, archaeological excavations yielded Aurignacian assemblages. The find layers occur at the southern base of a ridge composed of a mix of fine to coarse clastic sediments. Coarse and subangular material including small pebbles occurs at its base. Separated from the Vršac Mountains by a small depression, this ridge was likely formed as a tectonic push-up. Inside this ridge, coarser deposits (sand, gravels) of presently unknown facies occur, bearing rich archaeological assemblages that are thought to testify to the presence of the earliest modern humans in Europe some 40 ka ago (Mihailović, 2011; Chu *et al.*, 2014, 2016; Nett *et al.*, 2021).

Coring was conducted west-north-west of the archaeological sites (Fig. 1) in the large Alibunar Depression to obtain sediments for palaeoenvironmental reconstructions. The coring location was chosen after geophysical prospection by means of electrical resistivity tomography (ERT; Figs. 2 and S1–S3).

Methods

Electrical resistivity tomography and coring

ERT was conducted to detect stratigraphic differences within the near-surface Quaternary deposits and the underlying bedrock topography using a Syscal R1+ Switch 48 multielectrode device (Iris Instruments) and a Wenner-Schlumberger electrode array. Data were inverted incorporating the topography using the Res2Dinv inversion program (Geotomo Software). Three sediment cores were obtained by vibracoring. Steel augers (8 cm and 6 cm in diameter) were used in combination with an automotive drill rig (type Nordmeyer RS 0/2.3). Sediment cores were cleaned, photographed and described. Additional coring was conducted using closed auger heads (63 mm in diameter with a polypropylene liner of 50 mm diameter). The elevation and geographical position of all cores and ERT transects were measured using a differential GPS (type Topcon HiPerPRO).

Dating and age–depth model construction

Eight samples of polymineral fine grains (4–11 µm) were taken from halved sediment core VRT1A (diameter 5 cm, light-tight plastic liner), and were prepared for luminescence dating (Table 1) using conventional sample preparation techniques (Frechen *et al.*, 1996). All measurements were carried out on an automated Risø TL/OSL DA 20 reader equipped with a calibrated ^{90}Sr beta source using the post-infrared infrared stimulated luminescence signal measured at 290 °C (p-IR $IRSL_{290}$, Thiel *et al.*, 2011). Stimulation was carried out with infrared diodes (870 nm, FWHM = 40) and the signals were detected through an interference filter (410 nm). The initial 4 s of the signal minus a background of the last 20 s was used for p-IR $IRSL_{290}$ dating. Laboratory experiments included prior-IR stimulation temperature tests (Buylaert *et al.*, 2012) using a

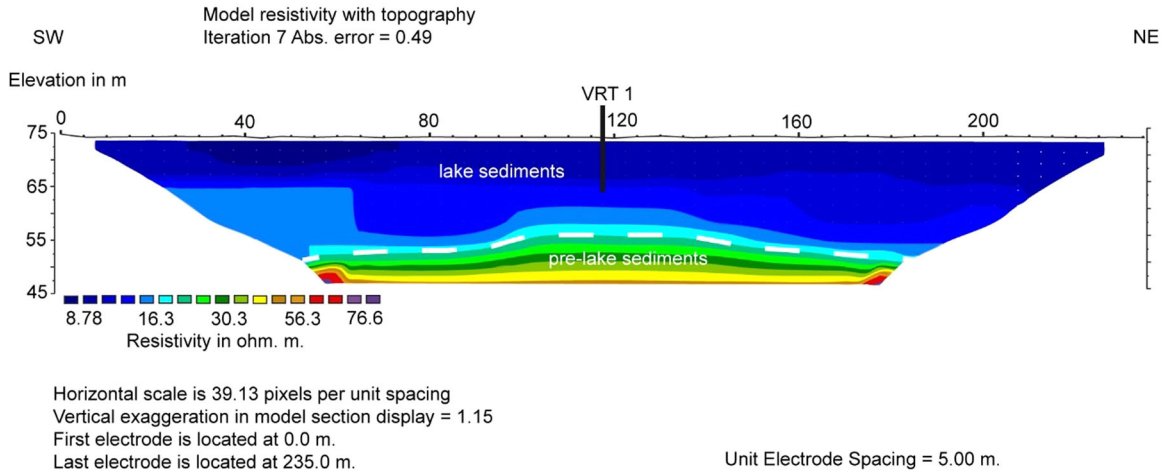

Figure 2. Inversion model of VRT ERT1 around the drill site (VRT1, for position see Supplement), showing that the core is situated in preferably undisturbed lacustrine sediment. Information on underlying sediments depicted by higher resistivity values (pre-lake sediments) is not available so far. The groundwater table is found in approx. 50 cm below ground surface. See Methods and Supplementary Materials for more detailed information on the methods and drill site description. [Color figure can be viewed at wileyonlinelibrary.com].

Table 1. Dose-rate data, equivalent dose values (9.8 mm aliquots) and $pIRIR_{290}$ ages. m b. s. = meters below surface; PM = polymineral fine grains; W% = measured water content (water mass over dry sediment mass); U = Uranium; Th = Thorium; K = Potassium; age calculation is based on cosmic dose calculation after Prescott and Hutton (1994), conversion factors of Guérin *et al.* (2011) and the measured water content; De = equivalent dose. The internal beta dose-rate contribution of the feldspar samples was calculated by assuming a potassium content of 12.5 ± 0.5% (Huntley and Baril, 1997).

Sample ID	Sample name	Sampling depth (m b.s.)	W (%)	Radionuclide concentration			IR_{50} g-value	$pIRIR_{290}$ g-value	IR_{50} Dose rate (Gy/ka)	$pIRIR_{290}$ Dose rate (Gy/ka)	IR_{50} De (Gy)	$pIRIR_{290}$ De (Gy)	IR_{50} Age (ka) corr	$pIRIR_{290}$ Age (ka) uncorr
				U (ppm)	Th (ppm)	K (%)								
C-L4029	VRT1-1	0.98	22	2.62 ± 0.48	13.1 ± 0.91	1.83 ± 0.20	2.56 ± 0.47	0.46 ± 0.15	3.87 ± 0.33	4.35 ± 0.33	58.9 ± 2.99	91.6 ± 4.81	19.5 ± 2.11	21.1 ± 1.93
C-L4422	VRT1A2	1.80	23	2.85 ± 0.31	14.6 ± 0.92	2.00 ± 0.15	2.28 ± 0.12	1.54 ± 0.53	4.18 ± 0.33	4.83 ± 0.36	105 ± 6.03	168 ± 8.99	31.5 ± 2.90	34.8 ± 3.22
C-L4423	VRT1A3	2.80	23	2.91 ± 0.33	14.2 ± 0.89	1.94 ± 0.15	2.39 ± 0.29	0.16 ± 0.09	4.09 ± 0.32	4.74 ± 0.36	145 ± 7.30	237 ± 12.6	45.0 ± 4.93	50.1 ± 4.66
C-L4424	VRT1A4	3.80	23	3.12 ± 0.34	14.6 ± 0.91	1.99 ± 0.15	2.03 ± 0.13	0.74 ± 0.16	4.23 ± 0.33	4.90 ± 0.37	145 ± 7.41	255 ± 13.1	42.0 ± 3.73	51.9 ± 4.79
C-L4030	VRT1-2	4.55	22	3.03 ± 0.51	13.6 ± 0.94	1.56 ± 0.17	2.83 ± 0.35	1.10 ± 0.20	3.77 ± 0.33	4.42 ± 0.34	204 ± 10.4	379 ± 20.2	73.0 ± 8.17	85.9 ± 7.97
C-L4031	VRT1-3	5.65	26	2.92 ± 0.66	13.7 ± 0.95	1.90 ± 0.15	2.83 ± 0.22	2.02 ± 0.34	3.87 ± 0.32	4.48 ± 0.37	295 ± 16.3	536 ± 27.1	103 ± 10.10	120 ± 11.605 m
C-L4032	VRT1-4	8.65	23	2.78 ± 0.48	14.1 ± 0.99	2.42 ± 0.26	-	-	-	4.99 ± 0.41	-	> 1150	-	> 230
C-L4033	VRT1-5	9.65	23	3.25 ± 0.57	13.8 ± 0.97	2.37 ± 0.25	-	-	-	5.11 ± 0.43	-	-	-	-

temperature range from 50 °C to 220 °C, and preheat plateau and dose-recovery tests. For the dose-recovery tests, the samples were illuminated for 24 h in a Hönle SOL2 solar simulator and a laboratory dose in the range of the natural dose was given to the samples, the prior-IR stimulation temperature was kept constant at 50 °C and the post-IR IRSL tracked the preheat temperature by −20 °C. The apparent residual dose after 24 h bleaching in the solar simulator was measured using routine measurements (Thiel *et al.*, 2011). Additionally, infrared stimulation measured at 50 °C (IR_{50}, Wallinga *et al.*, 2000; Preusser, 2003) was carried out for samples C-L4422 to C-L4424 and C-L4029 to C-L4031. Equivalent doses were calculated with an arithmetic mean. Fading tests (Auclair *et al.*, 2003) were carried out for all samples except C-L4032 and C-L4033 for both the IR_{50} and the p-IR-$IRSL_{290}$ measurement protocols. Only the IR_{50} ages were corrected for fading following the approach of Huntley and Lamothe (2001). The environmental dose rate was measured using high-resolution gamma-ray spectrometry. The dose rate was calculated with DRAC v.1.2 (Durcan *et al.*, 2015), using conversion factors of Guérin *et al.* (2011), an a-value of 0.12 ± 0.02 and the measured water content. The internal beta dose-rate contribution of the polymineral fine grain samples was calculated by assuming a potassium content of 12.5 ± 0.5% (Huntley and Baril, 1997). Alpha and beta attenuation factors of Bell (1980) and Mejdahl (1979) were used. The cosmic dose rate was calculated following Prescott and Hutton (1994).

The resulting IR_{50} and $pIRIR_{290}$ ages were used to construct an age–depth model. As we have no initial information on the depositional system and its homogeneity, we deliberately use the age–depth modelling approach of Zeeden *et al.* (2018), which does not make assumptions on sedimentation rates. This approach initially models the relative contributions of random and systematic uncertainty of an age dataset. This is done by using inversions as an indication of random uncertainty, and the lack of inversions as an indication of systematic uncertainty; it has been demonstrated to lead to realistic results (Zeeden *et al.*, 2018). In a second step, only the random uncertainty is used for an age–depth model. The systematic uncertainty is added again afterwards. In our opinion, this is the most robust method available for building reliable age models based on luminescence dates.

AMS ^{14}C dating of sediment bulk organic matter from two samples (depth: 2.2 m, 6.6 m) was carried out by BETA analytics. Samples were sieved, and the organic matter content of the < 180 µm fraction was exacted from the sediment and used for dating. This organic material did not include identifiable macroscopic remains. Calibration used the INTCAL13 database (Reimer *et al.*, 2013); results are displayed in Table 2.

Grain-size analysis

Granulometric analyses were carried out following the protocols of Schulte *et al.* (2016). The grain-size distribution was determined by applying the Mie theory (fluid refraction index (RI): 1.33; sample RI: 1.55; imaginary RI: 0, 1; Özer *et al.*, 2010; ISO 13320-1, 1999; *cf.* Schulte *et al.*, 2016). For details we refer to the Supplementary Data.

Ostracod analysis

Sediment material was screened for ostracod valves at eight discrete intervals. About 5 ml sediment was extracted from 1 cm segments and gently wet-sieved on a 150 µm screen. The residue was freeze-dried and ostracod valves were hand-picked under a stereo dissecting microscope. Identification keys and taxonomic

Table 2. ^{14}C dating results of two samples from core VRT1A. Calibration was done using the INTCAL 13 database.

Depth [m]	Lab code	Dated material	^{14}C age (yr BP)	1-σ uncertainty	Cal BP younger 2-σ boundary	Cal BP older 2-σ boundary
2.2	Beta-425214	organic sediment matter	8 460	30	9 450	9 525
6.6	Beta-425215	organic sediment matter	18 600	60	22 385	22 530

papers were used to identify the ostracod species and infer palaeoenvironmental conditions (Griffiths, 1995; Meisch, 2000; Mesquita-Joanes *et al.*, 2012).

Results

Electrical resistivity tomography and sediment coring

In general, inversion models of all ERT measurements show a two-partite structure of the subsurface with an upper unit of low resistivity values (between 6 Ωm and 16 Ωm) and a lower unit of increasing resistivities (~50 Ωm in VRT ERT 3, 77 Ωm in VRT 1 and 148 Ωm in VRT ERT 3; Figs. 2 and S1–S3). Only in VRT ERT 2, higher resistivity values around 30 Ωm occur close to the surface between 30 m and 65 m and between 120 m and 160 m of the measured transect in channel-like structures. The transition from lower to higher resistivities is observed in all ERT transects at a depth of 17–18 m below surface (b.s.), approximately 56–57 m amsl. In order to retrieve a preferably undisturbed sedimentary sequence, coring was conducted at 115 m of transect VRT ERT 1. Three cores were drilled in direct proximity to several decimetres at the drill site. The first core (VRT1) was cored as reconnaissance core with open augers to have control on the recovered sediments; it was drilled to a depth of 10.0 m. The second (VRT1A) and third (VRT1B) cores were drilled closed to a depth of 10.0 m (VRT1A) and 5.5 m (VRT1B; Figs. S4–S6), respectively. These were taken to obtain an overlapping composite record.

Figure 3 shows the sedimentary composition of vibracore VRT 1. Below the plough horizon, the upper part of the core (0.39–3.69 m, Fig. 3) is dominated by clay-rich silt and silt-rich clay of rusty greyish to greenish colours. While the upper ~2.00 m show low to moderate carbonate content, sediment from 2.00 m to 4.31 m is free of calcium carbonate. The sediment between 3.69 m and 4.71 m is characterised by darker greyish colours and increasing amounts of carbonates and mollusc detritus towards it base. A distinct shift in the sedimentary composition is visible at 4.71 m, where strongly decreasing clay content and a colour change towards light rusty grey was documented. This shift is not resolved by ERT measurements. The lower transition of these silt-dominated calcareous sediments occurs at 6.23 m. Below this level, the clay content increases and the carbonate content decreases again. The lower part of the core is again dominated by clay-rich silty sediments of rusty greyish to greenish colours. Only between 7.61 m and 8.33 m, slightly decreasing clay content accompanied by a change towards lighter greyish to brownish colours were documented. The overall fine-grained composition of the drill core is well reflected by VRT ERT 1 as the core is limited to the upper part of the low resistivity unit (between 6 Ωm and 16 Ωm, corresponding to clay and silty clay). Due to high drilling resistance, the transition to the underlying unit with increasing resistivity values, most likely corresponding to coarser-grained sediments, between 17 m b.s. and 18 m b.s. could not be reached.

Core VRT1A is similar to VRT1 in the stratigraphic build-up, but shows considerably more coring disturbance in the form of sediment smearing along the liners. A correlation based on visual core inspection is attempted in Fig. S4. In the uppermost core segment, the top 0.16 m are represented by an organic rich soil. Below, *c.* 0.08 m of relatively grey and clay-rich sediment occurs. From here downwards until *c.* 4.20 m b.s., clayey and rusty-greyish sediment occurs. In the interval from *c.* 2.40 m to 2.60 m, lighter sediment (with elevated carbonate content) is additionally present. From *c.* 4.30 m to 4.86 m, the sediment gradually becomes browner. Below ~4.86 m, lighter (ochre grey) and seemingly coarser sediment occurs again until ~9.50 m, where the sediment colour darkens again.

Core VRT1B shows similar patterns to core VRT1 and VRT1A (Figs. S5–S6). This core is less disturbed than core VTR1A. The uppermost core segment, drilled to 0.50 m b.s. to allow for overlapping sediment recovery, shows the recent/historic topsoil in the upper *c.* 0.16 m. This soil can be expected to be truncated due to activities connected with the drying of the area. Fine and clay-rich sediment of ochre-grey colour follows until about 3.80 m b.s., interbedded with a lighter and more carbonate-rich horizon at *c.* 2.15–2.30 m. From *c.* 3.80 m to 4.80 m the sediment becomes increasingly darker with three distinct carbonate-enriched intervals at *c.* 3.80 m, 4.10 m and 4.50 m depth, where carbonate concretions occur. Below ~4.80 m, lighter (ochre grey) and coarser sediment is again present until the end of the core at 5.50 m.

Stratigraphy by luminescence and ^{14}C dating

Figure 4A shows the luminescence and ^{14}C ages with depth; Tables 1 and 2 summarise the results. Laboratory doses were successfully recovered with a ratio of 1.02 ± 0.01 (sample C-L4029, n = 5); 1.03 ± 0.01 (sample C-L4030, n = 5); 1.07 ± 0.03 (sample C-L4422, n = 5); 1.02 ± 0.03 (sample C-L4423, n = 5); 1.01 ± 0.02 (sample C-L4424, n = 5) using the p-IR $IRSL_{290}$ protocol (Fig.S7). The laboratory experiment using different prior-IR stimulation temperatures indicated a plateau between 50 °C and 140 °C for samples C-L4029 and C-L4030 (Fig. S8). The prior-IR stimulation temperature of 140 °C did not reduce the p-IR $IRSL_{290}$ signal significantly and therefore we have chosen this prior-IR stimulation temperature for all further measurements (Fig.S9). A small residual dose of 6 Gy was left after 24 h of

Figure 3. Photo of vibracore VRT 1. Upper left corner = ground surface; lower right corner = final drilling depth (10 m b.s.). The core is dominated by silty sediments with various amounts of clay. Note the distinct shift from clay-rich dark greyish silts towards light-brown greyish silts with decreasing clay contents at 4.71 m. Photo P. Fischer (27.04.2015). [Color figure can be viewed at wileyonlinelibrary.com].

bleaching in the Hönle Sol2 solar simulator. This residual dose was not subtracted from the equivalent dose which is based on an arithmetic mean and was calculated to 91.6 ± 4.81 Gy (C-L4029, RSD = 3%), 168 ± 8.99 Gy (C-L4422, RSD = 6%), 237 ± 12.6 Gy (C-L4423, RSD = 4%), 255 ± 13.1 Gy (C-L4424, RSD = 4%), 379 ± 20.2 Gy (C-L4030, RSD = 5%) and 536 ± 27.1 Gy (C-L4031, RSD = 3%). Sample C-L4032 was close to saturation and has an equivalent dose (De) of > 1150 Gy, the p-IR $IRSL_{290}$ signal of sample C-L4033 is saturated. The measured fading rates (g_{2days}) are 0.46 ± 0.15% (n = 4, C-L4029), 1.54 ± 0.53% (n = 5, C-L4422), 0.16 ± 0.09% (n 5, C-L4423), 0.74 ± 0.16% (n = 5, C-L4424), 1.10 ± 0.20% (n = 4, C-L4030) and 2.02 ± 0.34% (n = 4, C-L4030). The equivalent dose was not corrected for anomalous fading. Luminescence age estimates based on p-IR $IRSL_{290}$ dating are 21.1 ± 1.93 ka, 34.8 ± 3.22 ka, 50.1 ± 4.66 ka, 51.9 ± 4.79 ka, 85.9 ± 7.97 ka, 120 ± 11.6 ka and > 230 ka (Table 1).

Laboratory doses were successfully recovered using IR_{50} stimulation with ratios of the measured to given dose of 0.95 ± 0.01 (n = 3, C-L4029), 0.97 ± 0.01 (n = 5, C-L4422), 0.97 ± 0.01 (n = 5, C-L4423), 0.96 ± 0.02 (n = 5, C-L4424), 0.89 ± 0.01 (n = 3, C-L4030), 0.89 ± 0.01 (n = 3, C-L4031), (Figs. S10 and S11). Equivalent doses were calculated with an arithmetic mean and resulted in 58.9 ± 2.99 Gy (n = 10, C-L4029), 105 ± 6.03 Gy (n = 10, C-L4422), 145 ± 7.30 Gy (n = 10, C-L4423), 145 ± 7.41 Gy (n = 10, C-L4424), 204 ± 10.4 Gy (n = 10, C-L4030), 295 ± 16.3 Gy (n = 10, C-L4031). Fading rates (g_{2days}) of 2.56 ± 0.47% (n = 5, C-L4029), 2.28 ± 0.12% (n = 5, C-L4422), 2.39 ± 0.29% (n = 5, C-L4423), 2.03 ± 0.13% (n = 5, C-L4424), 2.83 ± 0.35% (n = 5, C-L4030) and 2.83 ± 0.22% (n = 5, C-L4030) were measured. Luminescence age estimates of the fading corrected IR_{50} signal were calculated to 19.5 ± 2.11 ka, 31.5 ± 2.90 ka, 45.0 ± 4.93 ka, 42.0 ± 3.73 ka, 73.0 ± 8.17 ka, 103 ± 10.1 ka (Table 1).

Dating of sediment organic matter of two ^{14}C samples resulted in calibrated age ranges of 9450–9525 a cal BP at 2.2 m depth and of 22 385–22 530 a cal BP at 6.6 m depth (Table 2; Fig. 4).

An age–depth model builds a stratigraphic interpretation of optically stimulated luminescence (OSL) ages for the upper part of the core. Age increases almost linearly with depth (Fig. 4A).

Grain-size analysis

Figure 4B shows the grain-size distribution of the vibracore VRT 1. With the exception of several samples between 4.70 m and 7.70 m depth which are monomodal, the samples are poorly sorted and polymodal. However, each sample has a main mode or at least a subordinate mode within the middle- or coarse-silt fraction. For the sediments between 1.40 m and 4.20 m there is a distinct minor mode within the medium clay fraction visible. From 4.70 m to 6.10 m depth, the curve progression of the particle-size distribution has a single maximum at ~20 µm; the main modes show a fining upwards from 20 µm to 26 µm. Also, the sediments between 6.40 m and 7.70 m have mode values (15–20 µm) slightly shifted to the medium silt range. The samples between 8.70 m and 9.70 m are similar to the upper part between 1.40 m and 4.20 m, showing a distinct secondary mode within the clay fraction. Within the upper 4 m, the highest grain-size density varies between 6 µm and 9 µm, while the sediments of Unit 2 show fining upwards and reach considerably high values of 19 µm at a depth of 4.80 m. Above, and until *c.* 6 m, the sediment is coarser with a mode in grain size around 20 µm. Below, and until the base of the core, the sediment is fining towards a similar grain size to that in the upper part of the core. The submicron fraction (<1 µm) shows the lowest values around 8 vol% in the samples between 4.70 m and 6.10 m, and considerably high values (20 vol% to 26 vol%) from 4.30 m to 1.40 m and between 8.70 m and 9.70 m. The values of the upper part vary in a more moderate range (13 vol% to 17 vol%).

Ostracod analysis

Eight samples were analysed for ostracod valve occurrence. In general, the material was dominated by lacustrine species and

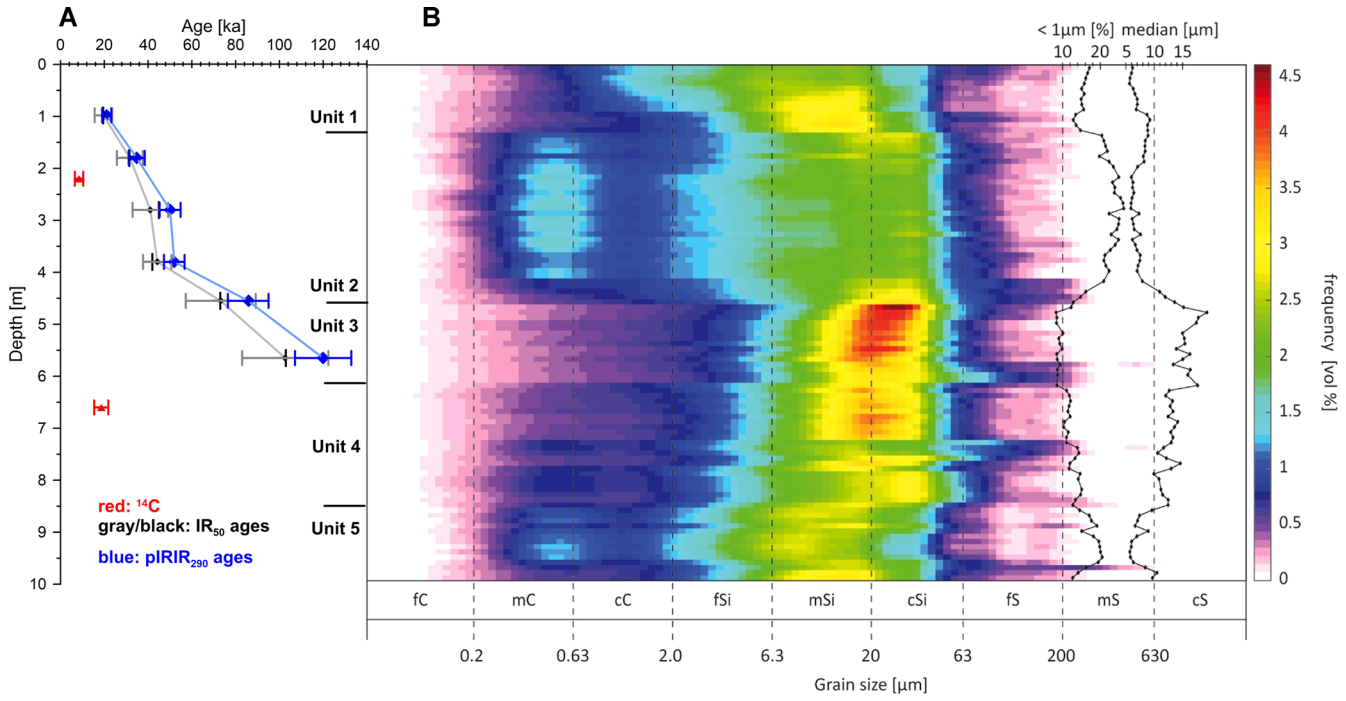

Figure 4. (A) Age-depth relationship of the Vršac core, and lithological units as discussed in chapter 5. Blue and grey lines and error bars represent the result of age-depth models based on pIRIR290 and IR50 ages, respectively. (B) Frequency distribution (heatmap) showing the grain size distribution of the samples from the VRT1 core as high contribution (red) and low contributions (white/blue colours), see scale at the right. The vertical curves represent the median (right) and the content of submicron particles (left). [Color figure can be viewed at wileyonlinelibrary.com].

here especially juvenile candonids, which were present in all samples that yield ostracod valves *per se* (Mesquita-Joanes *et al.*, 2012). The bottom-most sample at 9.3 m core depth is void of ostracod valves. The subsequent sample at 8.3 m core depth contains few valves of unidentifiable *Candona* sp. First, adult valves of *Candona neglecta* appear in the sample at 7.3 m core depth, complementing the juvenile fossil record of candonids. The fauna in the material from 6.3 m core depth holds well-preserved valves of adult *Candona neglecta* and *Candona* sp. The findings are supplemented by abundant valves of *Darwinula stevensoni*. Within the sample from 5.3 m core depth few valves of *Cyclocypris* sp. occur and further diversify the lacustrine species composition. The assemblage at 4.3 m core depth is dominated by *Ilyocypris* cf. *decipiens*. Accompanying species are *Candona neglecta* and *Candona* sp. The sample at 2.3 m sediment depth is again void of ostracod remains and the topmost sample yields only a single juvenile candonid valve.

Discussion

Sedimentology and stratigraphy

Vibracoring stopped at a depth of 10.0 m b.s. due to the stiffness of the sediments. The facies of the sediments underlying the lacustrine sediments remains unclear although ERT data indicate another *c.* 8.0 m of similar sediments. In contrast to VRT ERT 1, higher resistivity values close to the surface of VRT ERT 2 (see Fig. S2) indicate channel formation between 30 m and 60 m and are even more defined between 120 m and 160 m of the transect; these channels are most likely filled with coarser-grained sediments. In addition, the underlying deposits denominated as pre-lake sediments in Figs. 2, S2 and S3 show a surface dissected by a channel-like structure of low resistivity values, suggesting erosional processes prior to the deposition of fine-grained sediments in VRT ERT 2. In all ERT measurements, higher resistivity values of the lower unit indicate a change to coarser-grained sediments. The described shifts in grain size in correspondence with the observed stratigraphic sequence cannot be resolved by geoelectric measurements due to the decreasing sensitivity of ERT measurements with depth and overall small differences in grain size (Fischer *et al.*, 2016; Wunderlich *et al.*, 2018).

The cored Alibunar Basin north-west of Vršac reveals a sediment sequence forming the infill of a largely tectonically controlled local deposition centre, in which subsidence exceeds sediment input (as visible among others from the steep cliff at its western edge). Nonetheless, stratigraphic completeness and sedimentary continuity is likely but cannot be assured. The loess-like grain-size distributions (compare the density functions from aeolian loess from Krems in Sprafke *et al.*, 2020) at 4.7 m to 6.2 m and in the uppermost *c.* 1.4 m of the core, suggest a prevailing aeolian sediment input into an aquatic system. Also, sediment input directly from the catchment of short creeks draining the eastern fringe of the loess plateau at Alibunar or through erosion of the loess cliffs to the west of the depression may play a role. In between (*c.* 1.4–4.7 m) and below (from ~6.2 m downwards), the multimodal distribution including rather high amounts of clay suggests a complex sediment origin. Especially the high content of submicron material at 1.4–4.3 m depth indicates a lacustrine deposition environment, which has acted as a continuous trap for non-aeolian sediments, including a substantial part of suspended submicron particles. Submicron particles can either be deposited under prevailing still water conditions within an aquatic system (O'Melia, 1980; Torres *et al.*, 2005; Wilkinson and Lead, 2007; Dingman, 2009), may be part of autochthone bioproduction (diatoms, calcareous algae; the presence of these has not been investigated), or can originate from soil formation (Sun *et al.*, 2004, 2006). Because we do not see any reason for a discontinuous input of aeolian fine component, we interpret a detrital origin of these particles through the distal settlement of particles from superficial runoff (e.g. Torres *et al.*, 2005; Vandenberghe *et al.*, 2018) from the catchment. This includes a sediment component from the Banat Sands and also from the north-east and south, where erosion landforms and discharge structures are present and connected only to the basin. In general, grain-size distributions are similar to those from loess at Semlac in western Romania (Zeeden *et al.*, 2016), but are in most of the record supplemented by an additional finer component.

The ostracod assemblage clearly demonstrates a continuous lacustrine environment throughout the fossil record. We propose that the ostracod valves are partly transported due to the poor preservation condition or reflected by an incomplete ontogenetic record, where juvenile valves of *Candona* sp. are exclusively present in low abundance. High sedimentation rates and/or low oxygen availability at the sediment surface may also lead to a similar ostracod signal. A proper ontogenetic record is found in samples with dominating juvenile valves in relation to adult morphotype autochthonous populations, as in samples at 6.3 m, 5.3 m, and 4.3 m core depth. More specifically, we infer water temperature estimates from the Holarctic species, *Candona neglecta*, known from other reference studies (Viehberg, 2006). The species has a temperature optimum of about 4 °C during its final moulting time in springtime, while the juvenile forms can tolerate water temperatures of *c.* 20 °C and above (Meisch, 2000; Viehberg, 2006). Another dominating species is *Darwinula stevensoni*, a sediment-dwelling species with the ability to penetrate subaquatic seepages in lacustrine environments. The sporadic occurrence of *Cyclocypris* sp. hints at shallow water depth at the time of occurrence with an abundant macrophyte stand at the coring site (Meisch, 2000).

Based on the macroscopic core description and the available grain-size data, five lithological units can be discriminated: from top to ~1.20 m a silt dominated Unit 1 (#1); downwards to ~4.20 m a unit rich in fine clay follows (#2); below and from ~4.4 m down to *c.* 6.0 m, Unit 3 is similar to Unit 1 (#3). Unit 4 (#4) has the highest contribution of coarse silt and comprises the interval from ~4.4 m to 8.5 m. The lowermost Unit 5 is similar to Unit 2, and forms the base of the core (from ~8.5 m downwards; #5).

Challenges of age control

The chronological results of luminescence and radiocarbon dating contradict each other. While radiocarbon ages are < 23 ka for the upper 6.6 m, luminescence results increase constantly up to ~120 ka at 5.6 m depth. This suggests that either the radiocarbon samples are underestimated (e.g. through contamination by younger carbon via bioturbation or by carbon exchange via roots; Gocke *et al.*, 2017) or that the luminescence ages are overestimated (e.g. due to incomplete bleaching of the mineral grains before final deposition).

Two different luminescence dating measurement protocols were used, which generally agree with each other, although IR_{50} ages are consistently younger. Since these two signals bleach at different rates (i.e. signal resetting is faster for IR_{50} than for $pIRIR_{290}$; see also Veres *et al.*, 2018), their agreement suggests that the investigated grains have been completely bleached prior to sediment deposition. This would also be

expected from the depositional environment with a substantial part of suspended submicron particles from a distal source area and local runoff from the surrounding catchment that would have provided sufficient time for signal bleaching. The slight offset between both OSL datasets may be related to the fading correction of the IR_{50} signal or a slight overestimation of the $pIRIR_{290}$ signal, which was observed, e.g., in a Serbian loess–palaeosol sequence (Avram *et al.*, 2020). While one might argue that dating quartz minerals would be favourable in aquatic settings, since these bleach fast, it has already been demonstrated from the nearby investigation at the archaeological sites Crvenka-At (Nett *et al.*, 2021) that dating quartz in this basin is problematic. In-lake bleaching is probably dependent on how clear the lake is/how much light penetrates to the bottom.

For ^{14}C dating performed on bulk sediment, it is well known that this can include younger material from root channels or from sediment movement along cracks or pipes or directly from living roots (e.g. Gocke *et al.*, 2017). The measured 'soil organic matter' may be contaminated by younger carbon, which is known to lead to unrealistically young ages. The fact that ^{14}C ages show a low uncertainty which does not account for geological processes is well known (e.g. Telford *et al.*, 2004; Trachsel and Telford, 2017).

The luminescence ages suggest low average sedimentation rates of around 4 cm/ka during the last *c.* 25 ka, while the ^{14}C age model suggests much higher sedimentation rates of 20–25 cm/ka for the uppermost 2.2 m. Comparing this to aeolian sedimentation rates in the Banat at Orlovat (Lukić *et al.*, 2014; Marković *et al.*, 2014; Obreht *et al.*, 2015) and the Bačka loess plateau at Crvenka (Stevens *et al.*, 2011), the luminescence age model suggests rather low sedimentation rates for this depocentre. Such low sedimentation during the Upper Pleistocene is challenging to explain and sharply contradicts recent results obtained from the Kisiljevo LPS located upwind 50 km to the south (Perić *et al.*, in press). In contrast, the second ^{14}C date at 6.6 m depth implies rather high sedimentation rates.

When considering the ^{14}C ages as correct and extrapolating sedimentation rates to the lower part, the whole sequence would be formed during the last ~30–40 ka. This would imply similar sediment grain sizes during the Holocene (top), the LGM (~3–7 m) and the late last glacial cycle in the lower part. While ~3 m Holocene sediment fill may seem a reasonable accumulation comparable to other lacustrine geoarchives from the Carpathian Basin (e.g. Lake Fehér; Sümegi *et al.*, 2011a), the lack of a clear sedimentological shift from the LGM to the Holocene is intriguing. In such a scenario, the relatively coarse Unit 2 would date from ~18–13 ka, which does not relate to the LGM in the region (e.g. Sümegi *et al.*, 2012a; Magyari *et al.*, 2019) and is inconclusive or contradictory from a palaeoclimatic point of view. Grain sizes in our study are rather fine throughout, and also finer than at Semlac (Schulte *et al.*, 2014; Zeeden *et al.*, 2016), where loess-forming dust was suggested to be of non-local origin. Sümegi *et al.* (2011b, 2013b), however, reported lacustrine sedimentation rates from the Danube floodplain and Mureș (Maros) alluvial fan lakes similar to what ^{14}C ages suggest for the Vršac cores – but in minerogenic deposits with signs of high organic production and containing abundant fossils. Sümegi *et al.* (2011b) also report genetically similar sediments of loess deposited in an aquatic environment, and report sedimentation rates of ~7 cm/ka for these sediments – which is in the same order as that suggested by luminescence ages. On the other hand, the Fehér Lake (Sümegi *et al.*, 2011a), located only *c.* 150 km to the north-north-west, exhibits a similar lithofacies and an almost identical sedimentation rate when we rely on the obtained ^{14}C ages – but contains considerable amounts of autigenic carbonates and in-washed sediments (Sümegi *et al.*, 2011a), and may therefore be expected to exhibit higher sedimentation rates than the geoarchive under investigation here. The south-eastern part of the Alibunar Depression already has an area of > 100 km^2 and shows a catchment which also drains part of the Banat Sands. Lake level high stands are expected because of the presence of erosional cliffs in the loess west at Alibunar, indicating fluctuating lake levels.

While an age model based on the two available ^{14}C ages suggests a depositional history which is more similar to other much smaller lakes of oxbow character from the region, we are fully aware of issues with these. OSL ages suggest rather low sedimentation rates which are similar to dust accumulation in LPS plateau settings of the southern Carpathian Basin, but in contrast to recently obtained results from upwind LPS sites. Furthermore, low sedimentation rate scenarios do not favour an explanation that corroborates a lacustrine setting with a catchment of such a large dimension.

Sedimentological, palaeoenvironmental and archaeological implications

While the chronology is challenging, the grain-size data allow an interpretation regarding the palaeoenvironmental development, and thereby place the nearby archaeological sites (Chu *et al.*, 2014, 2016; Nett *et al.*, 2021) in a corresponding context. In addition, we discuss this geoarchive in the context of loess sedimentation.

Grain-size distributions are finest in Units 2 and 5, and considerably coarser in Unit 1 and especially Unit 3 (Fig. 4). In the Carpathian Basin, coarse aeolian grain sizes generally occur during glacials (e.g. Antoine *et al.*, 2009; Bokhorst *et al.*, 2011). Here we also expect an additional component of silt-sized (but not sand-sized) aquatic input, especially during high lake stands due to erosion in the catchment. While coarser grains would also be eroded, these were probably not transported to the centre of the depression, but were trapped by marginal lake vegetation. This aquatic component is expected to decrease during low lake stands because in this scenario input would not reach the centre of the depression.

Generally, environments during glacials are considered much dryer than during interglacials in the Eurasian loess belt (e.g. Heyman *et al.*, 2013; Sirocko *et al.*, 2016; Shao *et al.*, 2018). In the Carpathian Basin this is evidenced by negligible soil formation during peak glacials and weakly developed steppe soils during interstadials (e.g. Marković *et al.*, 2015, 2018). In contrast, warm interglacials experience strong soil formation. Consequently, high water tables in the depression are likely to be related to interglacial climates, and were less likely during interstadial periods. Also, autochthonous bioproduction is controlled by nutrient availability and temperature. In our opinion, Units 2 and 5 would relate to lake high stands, as evidenced by the clay which is probably related to distal settling. The erodibility of surface material is largely controlled by lake level and vegetation cover, which in turn depends on moisture. We propose that hinterland erosion took place predominantly during glacials when precipitation and lake level increased while vegetation cover was still restricted. This effect would be amplified by an extension of the catchment. The presence of fine sand in Units 3 and 4 is unlikely to be facilitated through riverine input in the depression centre, but is interpreted to be aeolian and may be the result of periods of enhanced storminess of the Košava wind system, as also suggested by their short duration (Fig. 4). In the relative vicinity, large dunes exist in the Banat Sands, demonstrating appropriate wind energy for sand transport

through the Košava wind system (Gavrilov *et al.*, 2018). Furthermore, long-range transport of sand particles has been demonstrated from the Atlantic (e.g. von Suchodoletz *et al.*, 2013; van der Does *et al.*, 2018), and is suggested to play a role here.

Following the luminescence age model (Fig. 4), Units 4 (to 5?) may be interpreted as the penultimate glacial phase and Unit 3 as corresponding to the last interglacial. Unit 2 may be related to the early Last Glacial (i.e. MIS 4–3), and Unit 1 would comprise the peak glacial and possibly the Holocene. Stratigraphy and environmental conditions reconstructed based on age models relying on the luminescence ages imply the opposite conclusions from those relying on geomorphological and sedimentological processes ruling the steppe environment of south-eastern Europe (e.g. Obreht *et al.*, 2019, and references therein). The OSL ages imply that the lake was more extended during glacial periods (Units 5 and 2) because the fine grain sizes related to distal settling from suspensions occur in these intervals, which contradicts the idea of rather dry glacials.

Our work relates the grain-size data to relative water table and to climate states. However, a definite connection to the established climate evolution of the Carpathian Basin (e.g. Marković *et al.*, 2015, 2018; Obreht *et al.*, 2019) cannot be made using either the ^{14}C or luminescence chronologies.

The implications of this past environmental reconstruction can provide context for the local Palaeolithic record that is otherwise known from loess and karstic deposits. Our ages are too insecure to make direct temporal connections with the modern human fossils and local Palaeolithic sites such as Crvenka-At. As a diachronic trend, Unit 2 suggests that the local lowlands were characterised by increasingly wet and diverse (representing fluvial, lacustrine, loess landscapes, dune environments) biomes during MIS 3 and we might begin to envision scenarios where these changing conditions may have impacted local Neanderthal biogeography (e.g. Mihailović, 2020). They may also have attracted intrepid modern humans that possibly had a broader dietary spectrum that may have included freshwater aquatic resources (Richards and Trinkaus, 2009; Trinkaus *et al.*, 2009). Behavioural changes in the Banat *c.* 40 ka ago, are marked by abrupt changes in lithic technology, but also in the size and location of archaeological sites. Sites in the lower elevations of the Banat show little or no evidence for earlier Middle Palaeolithic technology below the early Upper Palaeolithic assemblages, suggesting that modern human settlement in the area did not map directly onto those of earlier populations. However, whether these patterns were climatically controlled, either directly or indirectly, remains an aspect of future research. Especially helpful would be archaeological finds around 40 ka in a highly resolved palaeoclimate archive, where geophysical and geochemical proxies would allow sites to be placed directly into a palaeoclimatic context. Alternatively, precise and robust dating of both archaeological sites and palaeoclimate archives is needed to link these in an unambiguous manner.

Conclusions

The investigated sediment core near Vršac is a new continuous geoarchive, which serves for a better understanding of the Late Quaternary climate and environmental dynamics in the Carpathian Basin. The inferred results complement the known environmental reconstructions that derive mainly from loess–palaeosol sequences. The lacustrine sediment represents the first non-loess geoarchive from the region that potentially exceeds the last glacial period. Its sedimentation history and microfossil record provides insight into the past environment and interplay of lacustrine and aeolian sedimentation in a former freshwater lake.

Valuable/supplementary geoelectric analyses added stratigraphic information to the depositional environment/setting of the sediment basin. The geophysical prospection estimates the thickness to a total of *c.* 20 m sediment. A luminescence dating chronology of the upper half was established from drill core samples, but is contrasted by (only two) ^{14}C ages (Fig. 4A, Tables 1 and 2). Assumptions of sedimentation rates based on comparisons with other geoarchives from the region can aid an age interpretation. However, it challenges the concept of dry conditions during glacials and associated geomorphological and sedimentological processes.

Grain-size analysis results indicate fine sediment settling in a distal lacustrine environment from *c.* 1.4 m to 4.2 m and at the base of the core (below 7 m). In contrast, other intervals show grain-size distributions similar to aeolian sediments, suggesting their additional input into the lacustrine setting by winds or by fluvial erosion from the catchment of the depression. Comparison with a loess geoarchive from the region shows that the aeolian-deposited material is rather fine at this site, suggesting mostly non-local dust sources, and a transport range beyond local transport (Zeeden *et al.*, 2016), which is not typical for most thick loess–palaeosol sequences near the main dust sources in the Carpathian Basin (e.g. Basarin *et al.*, 2014; Obreht *et al.*, 2015). Our results suggest that in the vicinity (several km) of aeolian high-sedimentation areas which are dominated by local dust sources (Deliblatska Peščara), areas with low aeolian sedimentation coexist. This highlights that steppe landscapes in the Carpathian Basin are diverse and not solely loess-dominated, which is relevant for understanding early human environments and food sources.

Acknowledgements. The investigations were carried out in the context of the CRC 806 'Our way to Europe', subproject B1 'The Eastern Trajectory: Last Glacial Palaeogeography and Archaeology of the Eastern Mediterranean and of the Balkan Peninsula', and subproject F2 'Application of Luminescence and Electron-Spin-Resonance Dating Techniques in Geoarchaeological Contexts', funded by the Deutsche Forschungsgemeinschaft (DFG, German Research Foundation) – Projektnummer 57444011 – SFB 806. S.B.M. and M.B.G. acknowledge the financial support from grant 176020 of the Serbian Ministry of Education, Science and Technological Development. D.V. acknowledges support financed through the EEA-RO-NO-2018 Grant #0126 (KARSTHIVES2). We are grateful to Lea Obrocki and Jan Hošek for their help in the field. Radionuclide concentrations were measured using high purity germanium gamma spectrometry at VKTA Rossendorf (Dr D. Degering). Bruno Boemke, Janek Walk and Jonas Viehweger are thanked for support with maps. We thank the two reviewers for their constructive and helpful feedback. Open access funding enabled and organized by Projekt DEAL.

Supporting information

Additional supporting information may be found in the online version of this article at the publisher's web-site.

Figure S1: Position of ERT transects VRT 1-VRT 3 and vibracores VRT 1, VRT 1A, and VRT 1B.

Figure S2: Electric resistivity tomography image VRT 2 near the drill site.

Figure S3: Electric resistivity tomography image VRT 3 near the drill site.

Figure S4: Comparison and stratigraphic correlation of cores VRT1 (light, right core), VRT1A (leftmost core segments until 10 m), and VRT1B (middle core in the left panel).

Figure S4: Core images with depth scale of VRT1A. Gray parts are disturbed.

Figure S5: Core images with depth scale of VRT1B.

Figure S6: Dose recovery test of samples C-L4029, C-L4030, and C-L4422-4424. The preheat temperature was held constant at 320 °C using a $pIR_{140}IR_{290}$ stimulation. Samples were bleached in a Hönle Sol2 solar simulator for 24 h. The applied laboratory doses were in the range of the measured equivalent doses.

Figure S7: First IR stimulation temperature test of samples C-L4029 and C-L4030. The first IR stimulation temperature was increased between 50 °C and 140 °C, the pIRIR stimulation temperature was kept constant at 290 °C. A preheat plateau was observed between 50 °C and 140 °C for both samples.

Figure S8: Decay curve and dose response curve of sample C-L4424 using $pIR_{140}IR_{290}$ stimulation.

Figure S9: Decay curve and dose response curve of sample C-L4424 using IR_{50} stimulation.

Figure S10: Dose recovery test of samples C-L4029, C-L4030, and C-L4422-4424. The preheat temperature was held constant at 290 °C using an IR_{50} stimulation. Samples were bleached in a Hönle Sol2 solar simulator for 24 h. The applied laboratory doses were in the range of the measured equivalent doses.

Data availability statement

The data that support the findings of this study will be placed in the openly available PANGAEA database.

References Cited

Alex B, Mihailović D, Milošević S *et al*. 2019. Radiocarbon chronology of Middle and Upper Paleolithic sites in Serbia, central Balkans. *Journal of Archaeological Science: Reports* **25**: 266–279.

Anghelinu M, Niță L, Sitlivy V *et al*. 2012. Looking around Peștera Cu Oase: The beginnings of Upper Paleolithic in Romania. *Quaternary International* **274**: 136–157.

Antoine P, Rousseau D-D, Fuch M *et al*. 2009. High-resolution record of the last climatic cycle in the southern Carpathian Basin (Surduk, Vojvodina, Serbia). *Quaternary International* **198**: 19–36.

Auclair M, Lamothe M, Huot S. 2003. Measurement of anomalous fading for feldspar IRSL using SAR. *Radiation Measurements* **37**: 487–492.

Avram A, Constantin D, Veres D *et al*. 2020. Testing polymineral post-IR IRSL and quartz SAR-OSL protocols on Middle to Late Pleistocene loess at Batajnica, Serbia. *Boreas* **49**: 615–633.

Banak A, Mandic O, Sprovieri M *et al*. 2016. Stable isotope data from loess malacofauna: Evidence for climate changes in the Pannonian Basin during the Late Pleistocene. *Climate change in the Balkan-Carpathian region during Late Pleistocene and Holocene* **415**: 15–24.

Barbu S, Moisa C, Mircov VD 2009. *Cosava - a banatean wind*. Presented at the Research Journal of Agricultural Science, Agroprint; 365–371.

Basarin B, Buggle B, Hambac U *et al*. 2014. Time-scale and astronomical forcing of serbian loess-palaeosol sequences. *Global and Planetary Change* **122**: 89–106.

Bell WT. 1980. Alpha dose attenuation in quartz grains for thermoluminescence dating. *Ancient TL* **12**: 4–8.

Bokhorst MP, Vandenberghe J, Sümegi P *et al*. 2011. Atmospheric circulation patterns in central and eastern Europe during the Weichselian Pleniglacial inferred from loess grain-size records. *Quaternary International* **234**: 62–74.

Borić D, Dimitrijević V, White D *et al*. 2012. Early modern human settling of the Danube corridor: The Middle to Upper Palaeolithic site of Tabula Traiana Cave in the Danube Gorges (Serbia). *Antiquity* 86.

Buggle B, Hambach U, Glaser B *et al*. 2009. Stratigraphy, and spatial and temporal paleoclimatic trends in Southeastern/Eastern European loess–paleosol sequences. *Quaternary International* **196**: 86–106.

Buylaert J-P, Jain M, Murray AS *et al*. 2012. A robust feldspar luminescence dating method for Middle and Late Pleistocene sediments. *Boreas* **41**: 435–451.

Chu W. 2018. The Danube Corridor Hypothesis and the Carpathian Basin: Geological, Environmental and Archaeological Approaches to Characterizing Aurignacian Dynamics. *Journal of World Prehistory* **31**: 117–178.

Chu W, Hauck T, Mihailovic D. 2014. Crvenka-At– preliminary results from a lowland Aurignacian site in the middle Danube catchment. *In Palaeolithic and Mesolithic Research in the Central Balkans*. Belgrade: Serbian Archaeological Society 69–75.

Chu W, Mihailovic D, Pantovic I *et al*. 2016. Archaeological excavations at the fringe of Carpathian Basin (Vršac, Serbia). *Antiquity* **90**: 352.

Chu W, Pötter S, Doboș A *et al*. 2019. Geoarchaeology and geochronology of the Upper Palaeolithic site of Temerești Dealu Vinii, Banat, Romania: Site formation processes and human activity of an open-air locality. *Quartär* 111–134.

Dingman SL. 2009. *Fluvial hydraulics*. Oxford University Press: New York.

Does M, van der, Knippertz P, Zschenderlein P *et al*. 2018. The mysterious long-range transport of giant mineral dust particles. *Science Advances 4: eaau2* 768.

Durcan JA, King GE, Duller GAT. 2015. DRAC: Dose Rate and Age Calculator for trapped charge dating. *Quaternary Geochronology* **28**: 54–61.

Fenn K, Durcan JA, Thomas DSG *et al*. 2020. Re-analysis of late Quaternary dust mass accumulation rates in Serbia using new luminescence chronology for loess–palaeosol sequence at Surduk. *Boreas* **49**: 634–652.

Feurdean A, Perșoiu A, Tanțău I *et al*. 2014. Climate variability and associated vegetation response throughout Central and Eastern Europe (CEE) between 60 and 8 ka. *Quaternary Science Reviews* **106**: 204–224.

Fischer P, Wunderlich T, Rabbel W *et al*. 2016. Combined Electrical Resistivity Tomography (ERT), Direct-Push Electrical Conductivity (DP-EC) Logging and Coring – A New Methodological Approach in Geoarchaeological Research. *Archaeological Prospection* **23**: 213–228.

Fitzsimmons KE, Marković SB, Hambach U. 2012. Pleistocene environmental dynamics recorded in the loess of the middle and lower Danube basin. *Quaternary Science Reviews* **41**: 104–118.

Frechen M, Schweitzer U, Zander A. 1996. Improvements in sample preparation for the fine grain technique. *Ancient TL* **14**: 15–17.

Fu Q, Hajdinjak M, Moldovan OT *et al*. 2015. An early modern human from Romania with a recent Neanderthal ancestor. *Nature* **524**: 216–219.

Gavrilov MB, Marković SB, Schaetzl RJ *et al*. 2018. Prevailing surface winds in Northern Serbia in the recent and past time periods; modern- and past dust deposition. *Aeolian Research* **31**: 117–129.

Gocke MI, Huguet A, Derenne S *et al*. 2017. Disentangling interactions between microbial communities and roots in deep subsoil. *Science of the Total Environment* **575**: 135–145.

Griffiths HI. 1995. European Quaternary freshwater Ostracoda: a biostratigraphic and palaeobiogeographic primer, Ljubljana. Prirodoslovni muzej Slovenije.

Guérin G, Mercier N, Adamiec G. 2011. *Dose-rate conversion factors: update. Ancient TL* **29**: 5–8.

Haase D, Fink J, Haase G *et al*. 2007. Loess in Europe—its spatial distribution based on a European Loess Map, scale 1:2,500,000. *Quaternary Science Reviews* **26**: 1301–1312.

Heyman BM, Heyman J, Fickert T *et al*. 2013. Paleo-climate of the central European uplands during the last glacial maximum based on glacier mass-balance modeling. *Quaternary Research* **79**: 49–54.

Horváth F, Musitz B, Balázs A *et al*. 2015. Evolution of the Pannonian basin and its geothermal resources. *Geothermics* **53**: 328–352.

Huntley DJ, Baril MR. 1997. The K content of the K-feldspars being measured in optical dating or in thermoluminescence dating. *Ancient TL* **15**: 11–13.

Huntley DJ, Lamothe M. 2001. Ubiquity of anomalous fading in K-feldspars and the measurement and correction for it in optical dating. *Canadian Journal of Earth Sciences* **38**: 1093–1106.

Just J, Sagnotti L, Nowaczyk NR *et al*. 2019. Recordings of Fast Paleomagnetic Reversals in a 1.2 Ma Greigite-Rich Sediment Archive From Lake Ohrid, Balkans. *Journal of Geophysical Research: Solid Earth* **124**: 12445–12464.

Kels H, Protze J, Sitlivy V *et al*. 2014. Genesis of loess-like sediments and soils at the foothills of the Banat Mountains, Romania – Examples from the Paleolithic sites Românești and Coșava. *Quaternary International* **351**: 213–230.

Lehmkuhl F, Bösken J, Hošek J *et al*. 2018. Loess distribution and related Quaternary sediments in the Carpathian Basin. *Journal of Maps* **14**: 673–682.

Lehmkuhl F, Nett JJ, Pötter S *et al*. 2020. Loess landscapes of Europe – Mapping, geomorphology, and zonal differentiation. *Earth-Science Reviews* **215** 103496.

Lindner H, Lehmkuhl F, Zeeden C. 2017. Spatial loess distribution in the eastern Carpathian Basin: a novel approach based on geoscientific maps and data. *J. Maps* **13**: 173–181. https://doi.org/10.1080/17445647.2017.1279083

Lukić T, Basarin B, Buggle B *et al*. 2014. A joined rock magnetic and colorimetric perspective on the Late Pleistocene climate of Orlovat loess site (Northern Serbia). *Quaternary International* **334–335**: 179–188.

Magyari E, Buczkó K, Jakab G *et al*. 2009. Palaeolimnology of the last crater lake in the Eastern Carpathian Mountains: a multiproxy study of Holocene hydrological changes. *Hydrobiologia* **631**: 29–63.

Magyari EK, Veres D, Wennrich V *et al*. 2014. Vegetation and environmental responses to climate forcing during the Last Glacial Maximum and deglaciation in the East Carpathians: attenuated response to maximum cooling and increased biomass burning. *Quaternary Science Reviews* **106**: 278–298.

Magyari EK, Pál I, Vincze I *et al*. 2019. Warm Younger Dryas summers and early late glacial spread of temperate deciduous trees in the Pannonian Basin during the last glacial termination (20-9 kyr cal BP). *Quaternary Science Reviews* **225** 105980.

Marković SB, Oches EA, McCoy WD *et al*. 2007. Malacological and sedimentological evidence for "warm" glacial climate from the Irig loess sequence, Vojvodina, Serbia. *Geochemistry, Geophysics, Geosystems* **8**: Q09008.

Marković SB, Timar-Gabor A, Stevens T *et al*. 2014. Environmental dynamics and luminescence chronology from the Orlovat loess–palaeosol sequence (Vojvodina, northern Serbia). *Journal of Quaternary Science* **29**: 189–199.

Marković SB, Stevens T, Kukla GJ *et al*. 2015. Danube loess stratigraphy—Towards a pan-European loess stratigraphic model. *Earth-Science Reviews* **148**: 228–258.

Marković SB, Sümegi P, Stevens T *et al*. 2018. The Crvenka loess-paleosol sequence: A record of continuous grassland domination in the southern Carpathian Basin during the Late Pleistocene. *Palaeogeography, Palaeoclimatology, Palaeoecology* **509**: 33–46.

Marović M, Toljić M, Rundić L *et al*. 2007. *Neoalpine tectonics of Serbia*. Serbian Geological Society.

Matenco L, Radivojević D. 2012. On the formation and evolution of the Pannonian Basin: Constraints derived from the structure of the junction area between the Carpathians and Dinarides. *Tectonics* **31**: TC6007.

Meisch C. 2000. *Freshwater Ostracoda of Western and Central Europe*. Akademischer Verlag Spektrum: Heidelberg; 522.

Mejdahl V. 1979. Thermoluminescence Dating: Beta-Dose Attenuation in Quartz Grains. *Archaeometry* **21**: 61–72.

Mesquita-Joanes F, Smith AJ, Viehberg FA. 2012. Chapter 2 - The Ecology of Ostracoda Across Levels of Biological Organisation from Individual to Ecosystem: A Review of Recent Developments and Future Potential. In *Ostracoda as Proxies for Quaternary Climate Change, Developments in Quaternary Sciences*, Horne DJ, Holmes JA, Rodriguez-Lazaro J, Viehberg FA (eds). Elsevier, 15–35.

Mihailović D. 2020. Push-and-pull factors of the Middle to Upper Paleolithic transition in the Balkans. *Quaternary International* **551**: 47–62.

Mihailović D, Mihailović, B & Lopičić, M. 2011. The Palaeolithic in Northern Serbia. In *The Prehistory of Banat: The Palaeolithic and Mesolithic*, Tasić N, Drașovean F, Jovanović B (eds). Publishing House of the Romanian Academy: Bucharest. 77–101.

Molnár D, Hupuczi J, Galović L *et al*. 2010. Preliminary malacological investigation on the loess profile at Zmajevac, Croatia. *Central European Journal of Geosciences* **2**: 52–56.

Müller I. 1769. Mappa geographica novissima Regni Hungariae.

Müller UC, Pross J, Tzedakis PC *et al*. 2011. The role of climate in the spread of modern humans into Europe. *Quaternary Science Reviews* **30**: 273–279.

Nett JJ, Chu W, Fischer P *et al*. 2021. The early Upper Paleolithic site Crvenka-At, Serbia – the first Aurignacian lowland occupation site in the southern Carpathian Basin. *Frontiers in Earth Science* **9**: 56.

Obreht I, Hambach U, Veres D et al. 2017. Shift of large-scale atmospheric systems over Europe during late MIS 3 and implications for modern human dispersal. *Scientific Reports* **7**. https://doi.org/10.1038/s41598-017-06285-x

Obreht I, Zeeden C, Schulte P *et al*. 2015. Aeolian dynamics at the Orlovat loess–paleosol sequence, northern Serbia, based on detailed textural and geochemical evidence. *Aeolian Research* **18**: 69–81.

Obreht I, Zeeden C, Hambach U *et al*. 2016. Tracing the influence of Mediterranean climate on Southeastern Europe during the past 350,000 years. *Scientific Reports* **6** 36334.

Obreht I, Zeeden C, Hambach U *et al*. 2019. A critical reevaluation of palaeoclimate proxy records from loess in the Carpathian Basin. *Earth-Science Reviews* **190**: 498–520.

O'Melia CR. 1980. ES&T features: Aquasols: The behavior of small particles in aquatic systems. *Environmental Science & Technology* **14**: 1052–1060.

Özer M, Orhan M, IŞIK N. 2010. Effect of particle optical properties on size distribution of soils obtained by laser diffraction. *Environmental and Engineering Geoscience* **16**: 163–173.

Panagiotopoulos K, Aufgebauer A, Schäbitz F *et al*. 2013. Vegetation and climate history of the Lake Prespa region since the Lateglacial. *Quaternary International* **293**: 157–169.

Perić ZM, Marković SB, Avram A *et al*. in press. Initial quartz OSL and dust mass accumulation rate investigation of the Kisiljevo loess sequence in north-eastern Serbia. *Quaternary International* https://doi.org/10.1016/j.quaint.2020.10.040

Pigott J, Radivojević D. 2010. Seismic stratigraphy based chronostratigraphy (SSBC) of the Serbian Banat region of the Pannonian Basin. *Open Geosciences* **2**: 481–500.

Prescott JR, Hutton JT. 1994. Cosmic ray contributions to dose rates for luminescence and ESR dating: Large depths and long-term time variations. *Radiation Measurements* **23**: 497–500.

Preusser F. 2003. IRSL dating of K-rich feldspars using the SAR protocol: comparison with independent age control. *Ancient TL* **21**: 17–23.

Pross J, Koutsodendris A, Christanis K *et al*. 2015. The 1.35-Ma-long terrestrial climate archive of Tenaghi Philippon, northeastern Greece: Evolution, exploration, and perspectives for future research. *Newsletters on Stratigraphy* **48**: 253–276.

Reimer PJ, Bard E, Baylis A *et al*. 2013. IntCal13 and Marine13. *Radiocarbon Age Calibration Curves 0–50,000 Years cal BP. Radiocarbon* **55**: 1869–1887.

Richards MP, Trinkaus E. 2009. Isotopic evidence for the diets of European Neanderthals and early modern humans. *Proceedings of the National Academy of Sciences* **106**: 6034–16039.

Rudner ZE, Sümegi P. 2001. Recurring Taiga forest-steppe habitats in the Carpathian Basin in the Upper Weichselian. *Quaternary International* **76–77**: 177–189.

Schmidt C, Sitlivy V, Anghelinu M *et al*. 2013. First chronometric dates (TL and OSL) for the Aurignacian open-air site of Românești-Dumbrăvița I, Romania. *Journal of Archaeological Science* **40**: 3740–3753.

Schulte P, Lehmkuhl F, Kels H *et al*. 2014. Environmental change indicated by grain-size variations and trace elements: examples from two different sections - the sandy-loess sediments from the Doroshivtsy site (Ukraine) and the loess section Semlac (Romania). *Proscience* **1**: 106–112.

Schulte P, Lehmkuhl F, Steininger F *et al*. 2016. Influence of HCl pretreatment and organo-mineral complexes on laser diffraction measurement of loess–paleosol-sequences. *CATENA* **137**: 392–405.

Shao Y, Anhäuser A, Ludwig P *et al*. 2018. Statistical reconstruction of global vegetation for the last glacial maximum. *Global and Planetary Change* **168**: 67–77.

Sirocko F, Knapp H, Dreher F *et al*. 2016. The ELSA-Vegetation-Stack: Reconstruction of Landscape Evolution Zones (LEZ) from laminated Eifel maar sediments of the last 60,000 years. *Global and Planetary Change* **142**: 108–135.

Sitlivy V, Chabai V, Anghelinu M *et al*. 2012. The earliest Aurignacian in Romania: New investigations at the open air site of Românești-Dumbrăvița I (Banat). *Quartär* **59**: 85–130.

Sitlivy V, Chabai V, Anghelinu M *et al*. 2014. Preliminary reassessment of the Aurignacian in Banat (South-western Romania). *Quaternary International* **351**: 193–212.

Sprafke T, Schulte P, Meyer-Heintze S *et al*. 2020. Paleoenvironments from robust loess stratigraphy using high-resolution color and grain-size data of the last glacial Krems-Wachtberg record (NE Austria). *Quaternary Science Reviews* **248**: 106602.

Staubwasser M, Drăgușin V, Onac BP *et al*. 2018. Impact of climate change on the transition of Neanderthals to modern humans in Europe. *Proceedings of the National Academy of Sciences* **115**: 9116.

Stevens T, Marković SB, Zech M *et al*. 2011. Dust deposition and climate in the Carpathian Basin over an independently dated last glacial–interglacial cycle. *Quaternary Science Reviews* **30**: 662–681.

Suchodoletz H, von, Glaser B, Thrippleton T *et al*. 2013. The influence of Saharan dust deposits on La Palma soil properties (Canary Islands, Spain). *CATENA* **103**: 44–52.

Sümegi P, Lócskai T, Hupuczi J. 2011a. Late Quaternary palaeoenvironment and palaeoclimate of the Lake Fehér (Fehér-tó) sequence at Kardoskút (South Hungary), based on preliminary mollusc records. *Open Geosciences* **3**: 43–52.

Sümegi P, Molnár M, Jakab G *et al*. 2011b. Radiocarbon-dated paleoenvironmental changes on a lake and peat sediment sequence from the central Great Hungarian Plain (Central Europe) during the last 25,000 years. *Radiocarbon* **53**: 85.

Sümegi P, Gulyás S, Csökmei B *et al*. 2012a. Climatic fluctuations inferred for the Middle and Late Pleniglacial (MIS 2) based on high-resolution (ca. 20 y) preliminary environmental magnetic investigation of the loess section of the Madaras brickyard (Hungary). *Central European Geology* **55**: 329–345.

Sümegi P, Persaits G, Gulyás S. 2012b. Woodland-grassland ecotonal shifts in environmental mosaics: lessons learnt from the environmental history of the Carpathian Basin (Central Europe) during the Holocene and the last ice age based on investigation of paleobotanical and mollusk remains. In *Ecotones Between Forest and Grassland*. Springer; 17–57.

Sümegi P, Marković SB, Gulyás S *et al*. 2013a. Mollusc-based biogeographical data for refugee model of the Pannonian forest steppe. *Acta Biologica Cracoviensia*. Series Botanica. Supplement 1.

Sümegi P, Magyari E, Dániel P *et al*. 2013b. Responses of terrestrial ecosystems to Dansgaard–Oeshger cycles and Heinrich-events: A 28,000-year record of environmental changes from SE Hungary. *Quaternary International* **293**: 34–50.

Sun D, Bloemendal J, Rea DK *et al*. 2004. Bimodal grain-size distribution of Chinese loess, and its palaeoclimatic implications. *CATENA* **55**: 325–340.

Sun Y, Lu H, An Z. 2006. Grain size of loess, palaeosol and Red Clay deposits on the Chinese Loess Plateau: Significance for understanding pedogenic alteration and palaeomonsoon evolution. *Palaeogeography, Palaeoclimatology, Palaeoecology* **241**: 129–138.

Sušić Z, Toljić M, Bulatović V *et al*. 2016. Present-day Horizontal Mobility in the Serbian Part of the Pannonian Basin; Inferences from the Geometric Analysis of Deformations. *Acta Geophysica* **64**: 1629–1654.

Telford RJ, Heegaard E, Birks HJB. 2004. All age–depth models are wrong: but how badly? *Quaternary Science Reviews* **23**: 1–5.

Thiel C, Buylaert J-P, Murray A *et al*. 2011. Luminescence dating of the Stratzing loess profile (Austria) – Testing the potential of an elevated temperature post-IR IRSL protocol. *Quaternary International* **234**: 23–31.

Timár G, Székely B, Molnár G *et al*. 2008. Combination of historical maps and satellite images of the Banat region—re-appearance of an old wetland area. *Global and Planetary Change* **62**: 29–38.

Torres V, Vandenberghe J, Hooghiemstra H. 2005. An environmental reconstruction of the sediment infill of the Bogotá basin (Colombia) during the last 3 million years from abiotic and biotic proxies. *Palaeogeography, Palaeoclimatology, Palaeoecology* **226**: 127–148.

Tóth M, Buczkó K, Specziár A *et al*. 2018. Limnological changes in South Carpathian glacier-formed lakes (Retezat Mountains, Romania) during the Late Glacial and the Holocene: A synthesis. *Quaternary International* **477**: 138–152.

Trachsel M, Telford RJ. 2017. All age–depth models are wrong, but are getting better. *The Holocene* **27**: 860–869.

Trinkaus E, Moldovan O, Milota Ș *et al*. 2003. An early modern human from the Peștera cu Oase, Romania. *Proceedings of the National Academy of Sciences* **100**: 11231–11236.

Trinkaus E, Soficaru A, Doboș A *et al*. 2009. Stable isotope evidence for early modern human diet in southeastern. *Europe: Peștera cu Oase, Peștera Muierii and Peștera Cioclovina Uscată. Materiale Și Cercetări Arheologice* 4–14.

Trinkaus E, Bailey SE, Rougier H. 2012. *The dental and alveolar remains of Oase 1 and 2. Life and Death at the Pestera cu Oase: A Setting for Modern Human Emergence in Europe*. Oxford University Press: New York; 348–374.

Tzedakis PC, Hooghiemstra H, Pälike H. 2006. The last 1.35 million years at Tenaghi Philippon: revised chronostratigraphy and long-term vegetation trends. *Quaternary Science Reviews* **25**: 3416–3430.

Vandenberghe J, Sun Y, Wang X *et al*. 2018. Grain-size characterization of reworked fine-grained aeolian deposits. *Earth-Science Reviews* **177**: 43–52.

Veres D, Tecsa V, Gerasimenko N et al. 2018. Short-term soil formation events in last glacial east European loess, evidence from multi-method luminescence dating. *Quaternary Science Reviews* **200**: 34–51. https://doi.org/10.1016/j.quascirev.2018.09.037

Viehberg FA. 2006. Freshwater ostracod assemblages and their relationship to environmental variables in waters from northeast Germany. *Hydrobiologia* **571**: 213–224.

Wagner B, Vogel H, Francke A *et al*. 2019. Mediterranean winter rainfall in phase with African monsoons during the past 1.36 million years. *Nature* **573**: 256–260.

Wallinga J, Murray A, Duller G. 2000. Underestimation of equivalent dose in single-aliquot optical dating of feldspars caused by preheating. *Radiation Measurements* **32**: 691–695.

Wilkinson KJ, Lead JR. 2007. *Environmental colloids and particles: behaviour, separation and characterisation*. John Wiley & Sons.

Willis KJ, van Andel TH. 2004. Trees or no trees? The environments of central and eastern Europe during the Last Glaciation. *Quaternary Science Reviews* **23**: 2369–2387.

Willis KJ, Rudner E, Sümegi P. 2000. The Full-Glacial Forests of Central and Southeastern Europe. *Quaternary Research* **53**: 203–213.

Wunderlich T, Fischer P, Wilken D *et al*. 2018. Constraining electric resistivity tomography by direct push electric conductivity logs and vibracores: An exemplary study of the Fiume Morto silted riverbed (Ostia Antica, western Italy). *Geophysics* **83**: B87–B103.

Zech M, Buggle B, Leiber K *et al*. 2009. Reconstructing Quaternary vegetation history in the Carpathian Basin, SE-Europe, using n-alkane biomarkers as molecular fossils. *E&G – Quaternary Science Journal* **58**: 148–155.

Zeeden C, Hark M, Hambach U *et al*. 2007. Depressions on the Titel loess plateau: Form - Pattern - Genesis. *Geographica Pannonica* 4–8.

Zeeden C, Kels H, Hambach U *et al*. 2016. Three climatic cycles recorded in a loess-palaeosol sequence at Semlac (Romania) – Implications for dust accumulation in south-eastern Europe. *Quaternary Science Reviews* **154**: 130–142.

Zeeden C, Dietze M, Kreutzer S. 2018. Discriminating luminescence age uncertainty composition for a robust Bayesian modelling. *Quaternary Geochronology* **43**: 30–39.